Spin-charge separation and simultaneous spin and charge Kondo effect

Rok Žitko[1] and Janez Bonča[2,1]

[1]*J. Stefan Institute, Ljubljana, Slovenia*
[2]*Faculty of Mathematics and Physics, University of Ljubljana, Ljubljana, Slovenia*

(Dated: February 6, 2008)

We study the spin-charge separation in a Kondo-like model for an impurity with a spin and a charge (isospin) degree of freedom coupled to a single conduction channel (the "spin-charge" Kondo model). We show that the spin and charge Kondo effects can occur simultaneously at any coupling strength. In the continuum (wide-band or weak coupling) limit, the Kondo screening in each sector is independent, while at finite bandwidth and strong coupling the lattice effects lead to a renormalization of the effective Kondo exchange constants; nevertheless, universal spin and charge Kondo effects still occur. We find similar behavior in the two-impurity Anderson model with positive and negative electron-electron interaction and in the two-impurity Anderson-Holstein model with a single phonon mode. We comment on the applicability of such models to describe the conductance of deformable molecules with a local magnetic moment.

PACS numbers: 71.10.Ay, 71.10.Pm, 72.15.Qm, 71.38.-k

I. INTRODUCTION

Recent measurements of the transport properties of individual molecules using scanning tunneling spectroscopy, mechanically controllable break junctions, electromigration, and other methods have shown that the conductance strongly depends on electron-electron interaction as well as on the vibrational properties of electrode-molecule-electrode junctions, i.e. on the electron-phonon coupling[1,2,3,4,5,6,7,8,9,10]. On the theoretical side, the role of phonons had been studied in the framework of the Holstein[11,12] and Anderson-Holstein models[13,14,15,16,17,18,19,20,21,22], where the charge couples linearly to the displacement, and various models where the center-of-mass vibrations modulate the transparency of the tunneling barriers[23,24,25].

For sufficiently strong electron-phonon coupling of the Holstein type and for suitably tuned electrostatic potential (gate voltage), the low-energy electron configurations may consist of the empty and doubly occupied molecular orbital, while the singly occupied states are only virtually excited[14]. When these conditions are fulfilled, a charge equivalent of the Kondo effect occurs[14,15,16,26]. The effective pseudospin degree of freedom is in this case the axial charge[27] or isospin $I_z = 1/2(Q-1)$, where Q is the charge (level occupancy): empty orbital corresponds to isospin down, $I_z = -1/2$, while the doubly occupied orbital corresponds to isospin up, $I_z = +1/2$. The problem maps to the anisotropic charge Kondo model, where the impurity isospin couples to the isospin (charge and pairing) density of the conduction band via an isospin equivalent of the antiferromagnetic exchange interaction[15,26,28]. At low temperature the isospin is screened by pairing fluctuations in the conduction band and the ground state is a complex many-particle Fermi liquid state which is an isospin singlet. A $\pi/2$ phase shift occurs for low-energy quasiparticle scattering and the molecule becomes fully conductive when the temperature is reduced below the corresponding charge Kondo temperature T_K^C. In this respect, the charge Kondo effect is equivalent to the spin Kondo effect; the only difference are the interchanged roles of the isospin (charge and pairing) and spin degrees of freedom. We also remark that the charge Kondo screening of an isospin degree of freedom (electron *pairing moment*) is fundamentally different in its origin and its properties from the electrostatic screening of a point *charge* by the conduction electrons.

The Kondo model is an effective one-dimensional quantum field theory since the magnetic impurity is assumed to couple only to a one-dimensional continuum of conduction electron states with s symmetry about the impurity site[29]. Low-dimensional field theories have unique properties due to topological restrictions in reduced dimensionality; for example, fermions constrained to live on a 1D line can scatter only forwards and backwards. A notable effect in one-dimensional systems is the separation of electron spin and charge which had been intensively studied in Luttinger liquids[30]: fundamental low-energy excitations are not charged spin-$1/2$ Fermi-liquid quasiparticles, but rather spin-$1/2$ neutral particles (spinons) and charged spinless particles (holons). Such behavior has been found, for example, in one-dimensional solids such as $SrCuO_2$[31] and ballistic wires in GaAs/AlGaAs heterostructures[32].

Spin-charge separation also occurs in the Kondo problem. Using bosonization techniques, conduction band fermion fields can be described in terms of spin-up and spin-down boson fields. These bosons correspond to the particle-hole excitations in the conduction band and they can be recombined to form separate spin and charge fields which are essentially independent, but subject to a gluing condition[33,34] which is the only remnant of the charge-1, spin-$1/2$ nature of physical fermion particles. In the single-impurity spin Kondo problem, the impurity spin couples only to the spin field, while the charge field is decoupled[29,35,36]. In this sense, the spin and charge degrees of freedom are separated. As commented in Ref. 37, the spin-charge separation allows the quantization of spin to persist even in the case of strong coupling of a quantum dot to the leads when the charge is no longer quantized. This explains why unitary conductance can be achieved in quantum dots at relatively high (Kondo) temperature, which is essential for experimental observability of the Kondo effect in open quantum dots[38].

An interesting situation develops when one magnetic (spin)

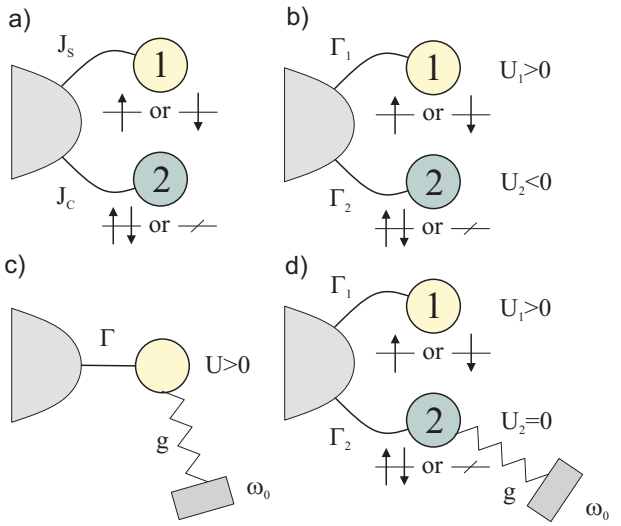

Figure 1: (Color online) Schematic representations of models discussed in the paper. a) Spin-charge Kondo model. b) Two-impurity Anderson model with positive and negative electron-electron interaction. c) Single-impurity Anderson-Holstein model. d) Two-impurity Anderson-Holstein model with electron repulsion in one orbital and electron-phonon coupling in the other.

Kondo impurity and one charge (isospin) Kondo impurity couple to the same conduction band, as schematically depicted in Fig. 1a. Due to the spin-charge separation, two Kondo screening cross-overs are expected to occur independently: the magnetic moment on the first impurity will be screened at the spin Kondo temperature $T_K^S \sim \exp(-1/\rho_0 J_S)$ [ρ_0 is the conduction band density of states at the Fermi level, J_S is the spin Kondo antiferromagnetic exchange constant] and the pairing moment (isospin) on the second impurity will be screened at the charge Kondo temperature $T_K^C \sim \exp(-1/\rho_0 J_C)$, where J_C is the charge Kondo exchange constant.

The goal of this paper is to corroborate the prediction of separate and independent spin and charge Kondo effects. We study how this scenario breaks down in the narrow bandwidth limit (large J_S/D and J_C/D) when lattice effects become important. We also study the related two-impurity Anderson model with one impurity with repulsive electron-electron interaction, $U > 0$, and one impurity with attractive interaction, $U < 0$, as we move away from the Kondo limit $|U|/\pi\Gamma \gg 1$ by increasing the hybridization strength Γ (see Fig. 1b). In the Anderson model, higher Γ implies stronger charge fluctuation on the magnetic ($U > 0$) site and stronger spin fluctuation on the isospin ($U < 0$) site.

The paper is organized as follows. In Sec. II we introduce the spin-charge Kondo model, describe its symmetries and comment on the possible symmetry-breaking terms. In Sec. III we present the numerical renormalization group (NRG) results for the thermodynamic quantities and study the degree of the spin-charge separation. In Sec. IV we study the model in the continuum (wide-band) limit using the non-Abelian bosonization to show how the spin and charge degrees of freedom separate, while in Sec. V we study the opposite limit of narrow bands. This naturally leads to the consideration of the strong-coupling fixed point in Sec. VI. The spin-charge separation in two-impurity Anderson models is studied in Sec. VII, while in Sec. VIII we comment on the effects of the simultaneous spin and charge Kondo effect on the transport through molecular junctions. This is supplemented in Sec. IX by an explicit demonstration of the charge Kondo effect in the two-impurity Anderson-Holstein model.

II. THE SPIN-CHARGE KONDO MODEL

The conventional spin Kondo model (SKM) is[39]

$$H_{\rm SKM} = \sum_{k\mu} \epsilon_k c^\dagger_{k\mu} c_{k\mu} + J_{\rm S} \boldsymbol{s}(0)\cdot\boldsymbol{S}, \tag{1}$$

where $J_{\rm S}$ is the antiferromagnetic Kondo exchange constant,

$$\boldsymbol{s}(0) = \frac{1}{2}\frac{1}{N_c^2}\sum_{kk'\mu\mu'} c^\dagger_{k\mu}\boldsymbol{\sigma}_{\mu\mu'}c_{k'\mu'} = \frac{1}{2}\sum_{\mu\mu'} f^\dagger_\mu \boldsymbol{\sigma}_{\mu\mu} f_{\mu'} \tag{2}$$

is the conduction-band spin density at the impurity site, where $\boldsymbol{\sigma}$ are the Pauli matrices, $c^\dagger_{k\mu}$ is creation operator for conduction-band electron with momentum k and spin μ, N_s is the number of states in the band, and $f^\dagger_\mu = 1/N_c \sum_k c_{k\mu}$ is the combination of the conduction band states which couples to the impurity. $\boldsymbol{S}$ is the impurity spin-$1/2$ operator. By analogy, the charge Kondo model (CKM) is[26]

$$H_{\rm CKM} = \sum_{k\mu} \epsilon_k c^\dagger_{k\mu} c_{k\mu} + J_{\rm C} \boldsymbol{i}(0)\cdot\boldsymbol{I}, \tag{3}$$

where $J_{\rm C}$ is the charge Kondo exchange constant,

$$\boldsymbol{i}(0) = \frac{1}{2}\frac{1}{N_c^2}\sum_{kk'\alpha\alpha'} \xi^\dagger_{k\alpha}\boldsymbol{\sigma}_{\alpha\alpha'}\xi_{k'\alpha'} \tag{4}$$

is the conduction-band isospin density at the impurity site and $\boldsymbol{I}$ is the impurity isospin-$1/2$ operator. Here $\xi^\dagger_{k\alpha} = \{c^\dagger_{k\uparrow}, c_{k\downarrow}\}$ is a Nambu spinor[40,41] for the conduction band electrons, so that

$$\begin{aligned}
i_x(0) &= \frac{1}{2}\frac{1}{N_c^2}\sum_{kk'}\left(c^\dagger_{k\uparrow}c^\dagger_{k'\downarrow} + c_{k\downarrow}c_{k'\uparrow}\right)\\
&= \frac{1}{2}\left(f^\dagger_\uparrow f^\dagger_\downarrow + f_\downarrow f_\uparrow\right)\\
i_y(0) &= \frac{1}{2}\frac{1}{N_c^2}\sum_{kk'}\left(-ic^\dagger_{k\uparrow}c^\dagger_{k'\downarrow} + ic_{k\downarrow}c_{k'\uparrow}\right)\\
&= \frac{1}{2}\left(-if^\dagger_\uparrow f^\dagger_\downarrow + if_\downarrow f_\uparrow\right)\\
i_z(0) &= \frac{1}{2}\frac{1}{N_c^2}\sum_{kk'}\left(c^\dagger_{k\uparrow}c_{k'\uparrow} + c^\dagger_{k\downarrow}c_{k'\downarrow} - \delta_{kk'}\right)\\
&= \frac{1}{2}\left(f^\dagger_\uparrow f_\uparrow + f^\dagger_\downarrow f_\downarrow - 1\right).
\end{aligned} \tag{5}$$

It should be noted that the z-component of the isospin density is the electron charge density measured with respect to

the half-filled band, while x and y-components are the electron pairing density. Contrary to the SKM, in CKM the impurity couples only to the charge sector of the conduction band, while the spin sector is decoupled (see Sec. IV).

We now combine the two models and introduce the spin-charge Kondo model (SCKM) with one spin impurity and one isospin impurity, both located at the origin:

$$H_{\rm SCKM} = \sum_{k\mu} \epsilon_k c^\dagger_{k\mu} c_{k\mu} + J_{\rm S} \boldsymbol{s}(0)\cdot\boldsymbol{S} + J_{\rm C}\boldsymbol{i}(0)\cdot\boldsymbol{I}. \quad (6)$$

An experimental realization of this model would consist of a single impurity with both charge and spin degrees of freedom, such as a deformable molecule embedded between two electrodes. In one possible scenario, two different molecular orbitals are active. One is singly occupied and has a magnetic moment localized, for example, on a magnetic ion embedded in a molecule. The other orbital is as an extended molecular orbital which is strongly coupled to a local phonon mode.

We remark that we have assumed the isospin part of the SCKM to be isotropic in spite of the fact that the Schrieffer-Wolff transformation applied to the Anderson-Holstein model in general yields an anisotropic effective exchange interaction[15,28]. The exchange anisotropy in spin-$1/2$ Kondo model is an irrelevant perturbation in the renormalisation group sense[42] and we disregard it in the first part of the paper, since it plays no role in the context of the spin-charge separation. The anisotropy can be, however, important in the experimental realizations of the model since it enters the expression for the charge Kondo temperature. We return to this point in Sec. IX.

The spin-charge Kondo model is distinct from the $\sigma - \tau$ Kondo model (also known as the compactified Kondo model)[36,43,44,45,46], where a single spin degree of freedom is coupled via $\boldsymbol{S}\cdot\boldsymbol{s}(0)$ and $\boldsymbol{S}\cdot\boldsymbol{i}(0)$ terms to a single conduction channel. In the compactified Kondo model, one takes advantage of the spin-charge decoupling and uses the additional isospin degrees of freedom in one channel to mimic the spin degrees of freedom of the second channel in the two-channel Kondo model. Our model features two different degrees of freedom, has different symmetry and thus different properties. Nevertheless, our results on the effects of the finite band-width (lattice effects) on the spin-charge separation help understand why the compactified Kondo model is not fully equivalent to the two-channel Kondo model (see also Refs. 43,46).

A. Symmetries and symmetry-breaking terms

We assume a linear dispersion relation $\epsilon_k = Dk$ for conduction band electrons, where $2D$ is the band-width and the wave-number k ranges from -1 to 1. The band is half filled (the chemical potential is at $\mu = 0$), so that we have particle-hole symmetry. The SCKM then has commuting $\mathrm{SU}(2)_{\rm spin}$ and $\mathrm{SU}(2)_{\rm isospin}$ symmetries generated by the spin and isospin operators

$$\begin{aligned} s^+ &= \sum_k c^\dagger_{k\uparrow} c_{k\downarrow} + S^+, \quad s^- = (s^+)^\dagger, \\ s^z &= \sum_k \frac{1}{2}\left(c^\dagger_{k\uparrow}c_{k\uparrow} - c^\dagger_{k\downarrow}c_{k\downarrow}\right) + S^Z, \\ i^+ &= \sum_k c^\dagger_{k\uparrow} c^\dagger_{k\downarrow} + I^+, \quad i^- = (i^+)^\dagger, \\ i^z &= \sum_k \frac{1}{2}\left(c^\dagger_{k\uparrow}c_{k\uparrow} + c^\dagger_{k\downarrow}c_{k\downarrow} - 1\right) + I^Z. \end{aligned} \quad (7)$$

In the presence of the magnetic field h and of detuned electrostatic potential δ, we add the following perturbation terms to the Hamiltonian:

$$H' = hS_z + \delta\,(Q-1) = hS_z + \delta\,(2I_z). \quad (8)$$

Magnetic field breaks the $\mathrm{SU}(2)_{\rm spin}$ symmetry, while detuned electric potential breaks the $\mathrm{SU}(2)_{\rm isospin}$ symmetry. Both perturbations are relevant: strong magnetic field $h > T_K^S$ quenches the spin Kondo effect, while strong potential $\delta > T_K^C$ quenches the charge Kondo effect.

III. NUMERICAL RESULTS

We studied the model using the well-established numerical renormalization group (NRG) technique[47,48]. We used an implementation of the NRG where the conservation of spin and isospin is explicitly taken into account.

We should emphasize the assumption of linear dispersion for conduction band electrons. It is known that in one-dimensional models spin and charge degrees of freedom truly separate only if the dispersion is exactly linear. The separation actually extends to the region of non-linear dispersion, however the spin and charge excitations acquire a finite lifetime[30,49,50,51]. By performing the calculations for a range of the discretization parameters Λ[48,52], we have verified that the results converge rapidly to the continuous band limit ($\Lambda \to 1$) and that the logarithmic discretization of the conduction band does not spoil the linearity. In this work we thus neglect the effects of non-linear conduction band dispersion, but we note that they could in fact also be studied using suitably adapted NRG code[53].

We computed the impurity contributions to the entropy and to the spin and charge susceptibilities. These thermodynamic quantities are defined as[54]

$$\begin{aligned} S_{\rm imp}(T) &= \frac{(E-F)}{T} - \frac{(E-F)_0}{T}, \\ \chi_{\rm spin}(T) &= \frac{(g\mu_B)^2}{k_B T}\left(\langle S_z^2\rangle - \langle S_z^2\rangle_0\right), \\ \chi_{\rm charge}(T) &= \frac{1}{k_B T}\left(\langle I_z^2\rangle - \langle I_z^2\rangle_0\right), \end{aligned} \quad (9)$$

where the subscript 0 refers to the situation when no impurities are present, $E = \langle H\rangle = \mathrm{Tr}\left(He^{-H/(k_BT)}\right)$, $F =$

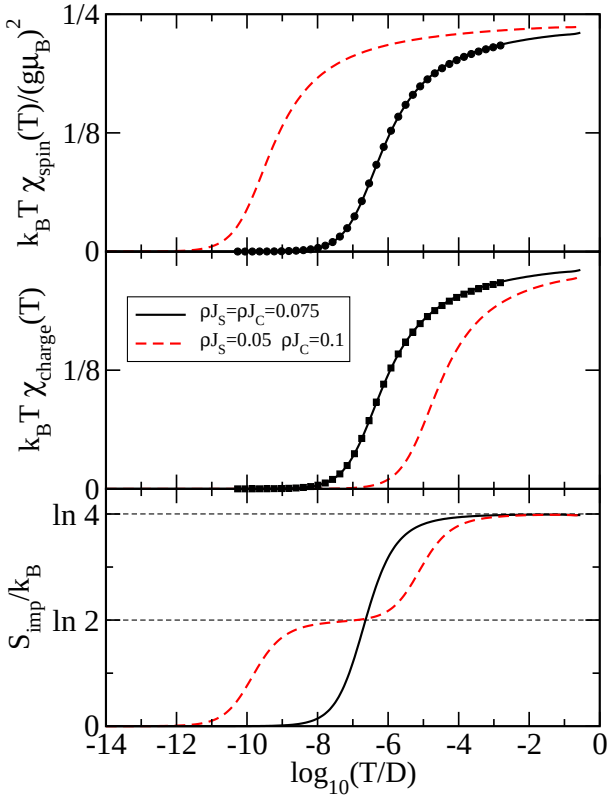

Figure 2: (Color online) Impurity susceptibilities and entropy for the spin-charge Kondo model. Filled symbols are a fit to the exact Bethe-Ansatz results for susceptibility. From this fit we deduce $T_K^S = T_K^C = 2.7 \times 10^{-7} D$, in approximate agreement with $T_K = D\sqrt{\rho J}\exp(-1/\rho J) = 4.4 \times 10^{-7} D$.

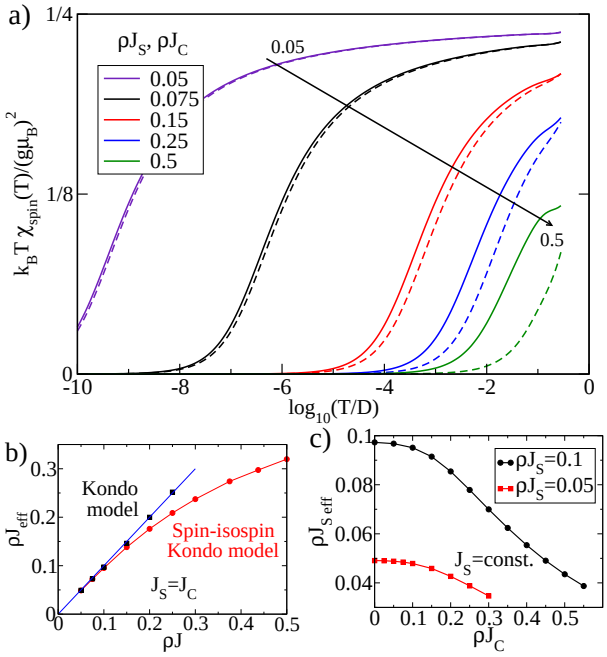

Figure 3: (Color online) a) Spin susceptibilities in the SCKM model with $J_C = J_S$ (solid lines) compared with spin susceptibilities in the corresponding SKM with the same Kondo exchange constant J_S (dashed lines). b) Effective exchange constant $J_{S\mathrm{eff}}$ as a function of J_S for the case $J_C = J_S$ (red, circles), compared with the single-impurity results (black, squares). Blue straight line is a fit to the single-impurity results and serves as a guide to the eye. c) Effective exchange constant $J_{S\mathrm{eff}}$ as a function of the charge Kondo exchange constant J_C while keeping the bare spin exchange constant J_S constant at $\rho J_S = 0.1$ (black, circles) or $\rho J_S = 0.05$ (red, squares).

$-k_B T \ln \mathrm{Tr}\left(e^{-H/k_B T}\right)$, g is the electronic gyromagnetic factor, μ_B the Bohr magneton and k_B the Boltzmann's constant.

We calculated these quantities as a function of the temperature for a number of choices of J_S and J_C, see Fig. 2. We used discretization parameters $\Lambda = 2, 3, 4$ and six different values of parameter z with the discretization scheme described in Ref. 52; the results nearly overlap for all three Λ. At each iteration we kept states up to an energy cut-off of at least $15T_N$, where T_N is the energy scale at the N-th iteration. Even-odd effects are removed by averaging over two consecutive iterations.

As expected, we observe Kondo screening of both spin and charge degrees of freedom. Kondo effects in each sector appear fully independent in the sense that the susceptibility curves χ_{spin} and χ_{charge} follow the universal $S = 1/2$ Kondo forms and each is characterized by a single parameter, the Kondo temperature T_K^S or T_K^C, respectively. Even for $J_S = J_C$, when the screening in each sector occurs at the same temperature, there is no competition between the two sectors and the curves agree perfectly with the exact Bethe-Ansatz results for the conventional $S = 1/2$ Kondo model (filled squares in Fig. 2).

On a lattice, spin and isospin cannot simultaneously be finite at one site[36,46]. We therefore expect that for large J_C and J_S, when the Kondo temperatures are high and the Kondo screening clouds are small, there should be some kind of mutual disturbance. We performed a series of calculations for increasing parameter $J = J_S = J_C$ and compared the spin susceptibility with that of a single-impurity spin Kondo model with the same J_S, see Fig. 3a. We find that the universality is maintained: for any J, the susceptibility still follows the universal Kondo curve. The Kondo temperature is, however, reduced in the spin-charge Kondo model and it is no longer accurately described by the familiar expression

$$T_K \approx D\sqrt{\rho J} e^{-\frac{1}{\rho J}}. \qquad (10)$$

A convenient quantity to study this renormalization effect are effective parameters $J_{S\mathrm{eff}}$ and $J_{C\mathrm{eff}}$, which can be obtained from respective Kondo temperatures T_K^S and T_K^C using the inverse of Eq. (10):

$$\rho J_{\mathrm{eff}} = \frac{2}{W[2/(T_K/D)^2]}, \qquad (11)$$

where $W(z)$ is the product logarithm function (the solution x of the equation $z = x\exp x$). In Fig. 3b we plot the $J_{S\mathrm{eff}}$ which corresponds to the susceptibility curves from Fig. 3a. For $J \ll D$ (i.e. in the wide-band limit), there is no renormalization and $J_{\mathrm{eff}} \approx J$. For $J \lesssim D$ we observe a systematic reduction of the effective exchange constant for increasing bare

J_S. This can be understood in terms of the "stiffness" of the Kondo clouds in spin and charge sector. With increasing J, the screening clouds are made to occupy smaller and smaller spatial extent around the impurity. Surprisingly, this does not lead to a collapse of the Kondo effects, as might be expected. Instead, the Kondo clouds spread out more than they do in the single impurity case to compensate for the conduction electron spin and isospin density loss due to the lattice effects.

In Fig. 3c we show the variation of $J_{S\text{eff}}$ for a constant bare J_S as the charge Kondo exchange J_C is increased from 0. The renormalization of the spin exchange constant is weaker for smaller bare J_S, when the spin Kondo cloud is more spread out, which confirms our interpretation in terms of interfering Kondo clouds.

IV. CONTINUUM (WIDE-BAND) LIMIT AND BOSONIZATION

The symmetry of the problem and the separation of the spin and charge sectors is directly exhibited in the non-Abelian bosonization approach of the boundary conformal field theory (CFT)[29,55]. The essence of this approach is to represent the electrons as independent bosonic fields carrying the isospin $\mathrm{SU}(2)$ and spin $\mathrm{SU}(2)$ degrees of freedom[45,56,57]. Introducing the left-moving field operators $\psi_\mu(x)$, we write the spin-charge Kondo Hamiltonian in real space as

$$\begin{aligned} H_{\mathrm{SCKM}} = \frac{iv_F}{2\pi}\sum_\mu \int_{-\infty}^{\infty} :\psi_\mu^\dagger(x)\frac{\partial\psi_\mu(x)}{\partial x}: \, dx \\ + v_F\rho\left(\lambda_S \boldsymbol{J}^S(0)\cdot\boldsymbol{S} + \lambda_C \boldsymbol{J}^C(0)\cdot\boldsymbol{I}\right), \end{aligned} \tag{12}$$

where v_F is the Fermi velocity, ρ is the density of states and $\boldsymbol{J}^S(x)$ and $\boldsymbol{J}^C(x)$ are spin and charge (isospin) "currents"[68] defined as

$$\begin{aligned} \boldsymbol{J}^S(x) &= \sum_{\mu\nu} :\psi_\mu^\dagger(x)\frac{1}{2}\boldsymbol{\sigma}_{\mu\nu}\psi_\nu(x):, \\ \boldsymbol{J}^C(x) &= \sum_{\alpha\beta} :\xi_\alpha^\dagger(x)\frac{1}{2}\boldsymbol{\sigma}_{\alpha\beta}\xi_\beta(x): \end{aligned} \tag{13}$$

where $\xi_\alpha^\dagger(x) = \left\{\psi_\uparrow^\dagger(x), \psi_\downarrow(x)\right\}$ is the real-space Nambu spinor. Normal ordering (double dots) has been introduced to remove divergences due to filled electron levels below the Fermi level. Note also that in this section the spin and charge Kondo coupling constants are λ_S and λ_C.

The Sugawara form[58] equivalent to the Hamiltonian Eq. (12) is[56,57]

$$\begin{aligned} H_{\mathrm{SCKM}} = \frac{\pi v_F}{l}\left[\frac{1}{3}\sum_n :\boldsymbol{J}^S_{-n}\cdot\boldsymbol{J}^S_n: + \frac{1}{3}\sum_n :\boldsymbol{J}^C_{-n}\cdot\boldsymbol{J}^C_n:\right] \\ + \frac{\pi v_F}{l}\left(\lambda_S\sum_n \boldsymbol{J}^S_n\cdot\boldsymbol{S} + \lambda_C\sum_n \boldsymbol{J}^C_n\cdot\boldsymbol{I}\right). \end{aligned} \tag{14}$$

Here $\boldsymbol{J}^S_n$ and $\boldsymbol{J}^C_n$ are the Fourier modes of the real-space currents $\boldsymbol{J}^S(x)$ and $\boldsymbol{J}^C(x)$ in a finite system of length $2l$. They each satisfy $\mathrm{SU}(2)_1$ Kac-Moody commutation relations

$$[J^{S/C,a}_n, J^{S/C,b}_m] = i\epsilon_{abc}J^{S/C,c}_{n+m} + \delta_{ab}\delta_{n+m,0}\frac{1}{2}n, \tag{15}$$

where ϵ^{abc} is the antisymmetric tensor[56]. The modes from different sectors commute:

$$\left[J^{S,a}_n, J^{C,b}_m\right] = 0. \tag{16}$$

This commutation relation embodies the (trivial) spin-charge separation of the free electrons ($\lambda_S = \lambda_C = 0$). At a special value $\lambda_S = 1/3$, we can introduce a new current $\vec{\mathcal{J}}^S = \boldsymbol{J}^S + \boldsymbol{S}$ which satisfies the same Kac-Moody commutation relations as the old currents. The spin part of the Hamiltonian then becomes (up to a constant term)

$$H^{(S)}_{\mathrm{SCKM}} = \frac{\pi v_F}{l}\sum_n \frac{1}{3} :\vec{\mathcal{J}}^S_{-n}\cdot\vec{\mathcal{J}}^S_n:, \tag{17}$$

from which the spin impurity $\boldsymbol{S}$ has disappeared (it was "absorbed" by the conduction band). The charge sector remains unaffected by this change. By analogy, at a special value $\lambda_C = 1/3$ we introduce $\vec{\mathcal{J}}^C = \boldsymbol{J}^C + \boldsymbol{I}$ and write the charge part of the Hamiltonian as

$$H^{(C)}_{\mathrm{SCKM}} = \frac{\pi v_F}{l}\sum_n \frac{1}{3} :\vec{\mathcal{J}}^C_{-n}\cdot\vec{\mathcal{J}}^C_n:, \tag{18}$$

The special values $\lambda_S = 1/3$, $\lambda_C = 1/3$ are identified with the strong coupling fixed point of the problem[29]. Note that

$$\left[\vec{\mathcal{J}}^{S,a}_m, \vec{\mathcal{J}}^{C,b}_n\right] = 0, \tag{19}$$

therefore the addition of the impurities does not break the spin-charge separation.

Even though the spin Kondo effect occurs in the spin sector, without involving the charge sector, and the charge Kondo effect occurs in the charge sector, without involving the spin sector, the spin and charge degrees of freedom are not entirely decoupled; they are constrained by the gluing condition. The gluing condition declares which combinations of quantum numbers are allowed taking into account the charge-1 spin-1/2 nature of physical particles – electrons. In the present context the gluing condition depends on the boundary conditions (b. c.) imposed on the field $\psi(x)$.

We first consider the case of anti-periodic b. c., $\psi(l) = -\psi(-l)$. We can obtain half-integer spin only with an odd number of electrons (i.e. for half-integer isospin)[29]. Therefore $2I^z$ and $2S^z$ must have the same parity; this is the gluing condition. There are thus two Kac-Moody conformal towers with highest-weight states having $(I, S) = (1/2, 1/2)$ and $(I, S) = (0, 0)$, respectively.

For periodic b.c. $\psi(l) = \psi(-l)$, and keeping in mind that the z-component of the isospin is defined with respect to half filling, we obtain half-integer spin for integer isospin and integer spin for half-integer isospin; $2I^z$ and $2S^z$ must

then have different parity. There are two conformal towers, $(I,S)=(1/2,0)$ and $(I,S)=(0,1/2)$. Note that changing the b. c. from periodic to anti-periodic (or vice versa) amounts to imposing a phase shift of $\pi/2$ on the wave function[55].

In the single impurity Kondo model, the finite-size spectrum of the strong coupling fixed point is obtained by a fusion in the spin sector[29,55]. This means that the isospin sector remains intact, while the spin quantum number changes as $S \to 1/2 - S$. As a consequence $(1/2,1/2) \to (1/2,0)$ and $(0,0) \to (0,1/2)$, i.e. the gluing conditions change from those for the anti-periodic b. c. to those for periodic b. c., and vice versa, which is equivalent to the $\pi/2$ phase shift.

We now generalize this fusion rule to the case of both (spin and isospin) impurities. The absorption of the spin impurity will not affect the isospin sector ($I \to I$), however $S \to 1/2 - S$. Similarly, the absorption of the isospin impurity does not affect the spin sector $S \to S$, while $I \to 1/2 - I$. The fusion rule is thus $S \to 1/2 - S$ and $I \to 1/2 - I$. Therefore $(0,0) \to (1/2,1/2)$ and $(1/2,1/2) \to (0,0)$ for periodic b.c. and $(1/2,0) \to (0,1/2)$ and $(0,1/2) \to (1/2,0)$ for anti-periodic b.c.: the boundary conditions remain the same, only the conformal towers are permuted. There is no phase shift in this case. Alternatively, we can consider the fusion in each sector to give a $\pi/2$ phase shift. This gives a total phase shift of π which, however, is equivalent to zero phase shift since phase shifts are defined modulo π. The finite-size spectrum is that of free fermions, therefore the fixed point corresponds to a Fermi liquid.

V. ZERO-BANDWIDTH AND NARROW-BAND LIMITS

For very large J_C and J_S, SCKM reduces to the zero-bandwidth limit where the band is effectively described as a single orbital. In this three-site problem, the ground state for $J_S > J_C$ is a spin singlet + a free isospin, while for $J_C > J_S$ the ground state is an isospin singlet + a free spin. Spin and isospin are in direct competition since a single band "orbital" can either behave as a spin degree of freedom or as an isospin degree of freedom, but not both at the same time. Only one of the two possible Kondo ground states can be realized.

At finite bandwidth additional degrees of freedom become available and the spin and charge Kondo effects can occur simultaneously. In the next approximation, we therefore take two lattice sites to mimic the conduction band. This "narrow-band limit" is the minimal model for a band with independent spin and isospin degrees of freedom. We use $H_{\rm band} = -t\sum_\mu c^\dagger_{1\mu}c_{0\mu}$ + H.c., where $t \ll J_C, J_S$. In this approximation the ground state is spin-singlet isospin-singlet for any values of J_C and J_S, as expected. The ground state energy is

$$E_{\rm GS} = -\frac{3}{8}\left(J_C + J_S + \sqrt{(J_C - J_S)^2 + \left(\frac{8}{3}\right)^2 t^2}\right). \tag{20}$$

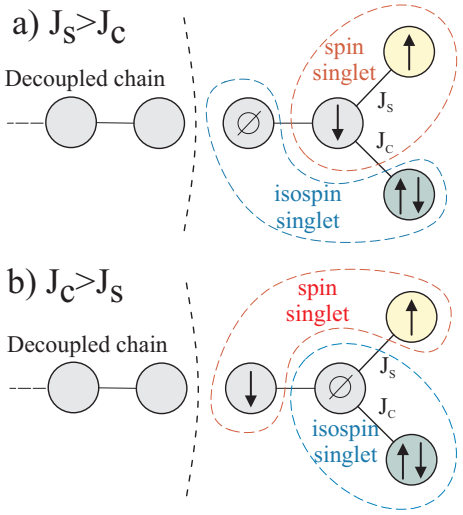

Figure 4: (Color online) Schematic representation of the strong coupling fixed point Hamiltonian of the spin-charge Kondo model for a) $J_S > J_C$ and b) $J_C > J_S$. For $J_C = J_S$, the fixed point corresponds to the symmetric combination of a) and b).

which, for large $J_S/t, J_C/t$, equals

$$E_{\rm GS} \sim \begin{cases} -\frac{3}{4}\max\{J_C, J_S\} - \frac{4}{3}\frac{t^2}{|J_C - J_S|} & \text{if } |J_C - J_S| \gg t, \\ -\frac{3}{4}J - t & \text{if } |J_C - J_S| \ll t. \end{cases} \tag{21}$$

In the second line $J \sim J_C \sim J_S$. The fixed point Hamiltonian consists of the impurity sites strongly coupled to the first two sites of the Wilson chain, which thereby become decoupled from the remainder of the chain.

VI. FIXED POINTS

In the single-impurity Kondo model with one spin (isospin) impurity, the strong coupling fixed point corresponds to the impurity site and the first site of the Wilson chain being tightly bound into a spin (isospin) singlet, which results in the decoupling of the first site of the Wilson chain from the rest[47,48]. As a result, the low-energy electrons experience a $\pi/2$ scattering phase shift. As shown in the previous section, in the strong coupling fixed point of the SCKM two sites are removed from the chain (see Fig. 4). This corresponds to a zero phase shift for quasiparticles, in agreement with the CFT analysis.

The $\mathrm{SU}(2)_{\rm spin} \times \mathrm{SU}(2)_{\rm isospin} \simeq \mathrm{O}(4)$ symmetry with zero phase shift of the SCKM model should be contrasted with the $\mathrm{O}(3) \times \mathrm{O}(1)$ symmetry of the $\sigma - \tau$ model at its NFL fixed point or the $\mathrm{O}(4)$ symmetry with $\pi/2$ phase shift at its FL fixed point when an anisotropy between spin and isospin sectors exists[43,45].

VII. SPIN-CHARGE SEPARATION IN THE TWO-IMPURITY ANDERSON MODEL

The Kondo model is an effective low-temperature theory of a magnetic impurity. If the physical reality is modelled more accurately, the impurity is described using the single impurity Anderson model (SIAM)[59] and the Kondo model arises only as a low-temperature effective theory of SIAM after the charge-fluctuations are projected out using the Schrieffer-Wolff transformation[60]. In SIAM, charge fluctuations persist at low temperatures and, in fact, they must be present since they provide the mechanism by which the impurity spin can flip. Nevertheless, in the strong Kondo regime, $U/\pi\Gamma \gg 1$ (where U is the electron repulsion and Γ the hybridization strength), the Anderson impurity still couples predominantly to the spin sector of the conduction band and only weakly to the charge sector. In fact, this problem has to be considered from the renormalization group point of view. At high energy (temperature), when the system is in the free-orbital regime, the impurity indeed couples to both spin and charge sectors. At low energy, when the system is in the local moment regime, the coupling to the charge sector is frozen out. This implies that the spin and charge separate only for low energy electrons, while the two degrees of freedom are "entangled" for high energy electrons. Due to the energy-scale separation in quantum impurity models[47], the lack of the spin-charge separation at high energies does not preclude the spin-charge separation at low energies (i.e. at low temperatures). Alternatively, this can be phrased in terms of the separation of time scales[54]: the duration of fluctuations (spin flips) is $\tau_U \sim \hbar/U$ while the "magnetic" time scale (roughly equivalent to the mean time between successive spin flips) is $\tau_K \sim \hbar/T_K$. In the Kondo limit, $T_K \ll U$ and therefore $\tau_K \gg \tau_U$.

In the Anderson model with negative U the spin and charge sectors are interchanged[26]. For temperatures below $|U|$, a pairing moment develops in place of the magnetic moment. The impurity state can be flipped from zero-occupancy (isospin down) to double-occupancy (isospin up) by coupling to the conduction band. The single-occupancy states can be projected out using a suitably generalized Schrieffer-Wolff transformation and the effective model is the charge (isospin) Kondo model[26].

Generalizing the spin-charge Kondo model, we now study the two-impurity Anderson model (2IAM) described by the Hamiltonian

$$\begin{aligned} H = &\sum_{k\sigma} \epsilon_k c^\dagger_{k\sigma} c_{k\sigma} + \frac{U_1}{2}(n_1-1)^2 + \delta_1(n_1-1) \\ &+ \frac{U_2}{2}(n_2-1)^2 + \delta_2(n_2-1) \\ &+ \sum_{k\sigma} V^1_k \left(d^\dagger_{1\sigma} c_{k\sigma} + \text{H.c.} \right) + \sum_{k\sigma} V^2_k \left(d^\dagger_{2\sigma} c_{k\sigma} + \text{H.c.} \right). \end{aligned} \tag{22}$$

Here $n_i = \sum_\sigma d^\dagger_{i\sigma} d_{i\sigma}$ is the electron occupancy of impurity i, $U_1 > 0$ is the electron-electron (e-e) repulsion on impurity 1, $U_2 < 0$ is the e-e attraction on impurity 2. We assume a constant hybridization strength $\Gamma = \pi\rho_0 |V_{k_F}|^2$; this permits

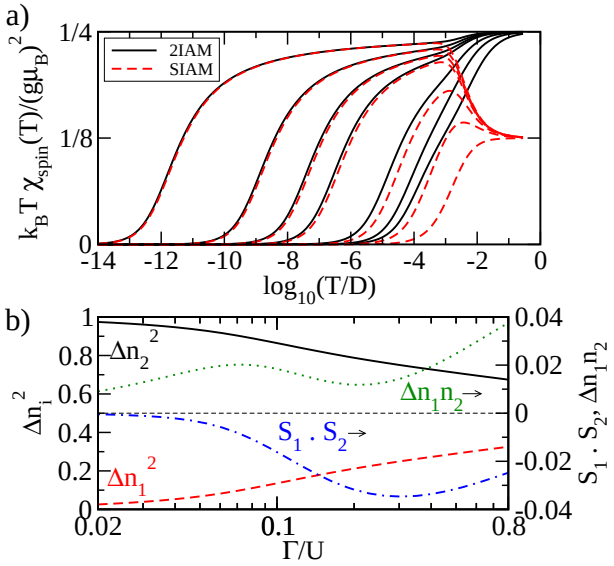

Figure 5: (Color online) a) Spin susceptibility for 2IAM (full lines). We choose $U_1 = -U_2 = U$ and $\Gamma_1 = \Gamma_2 = \Gamma$. For comparison we plot results of the SIAM with the same Γ and U (dashed lines). Parameters are $U/D = 0.01$ and $\Gamma/U = 0.02, 0.03, 0.04, 0.05, 0.1, 0.2$ and 0.5 (left to right). b) Charge fluctuations and correlations in 2IAM for increasing hybridization strength Γ.

comparison with the Kondo model which, in a similar manner, has a constant density of state ρ_0 and a constant exchange constant J_K (this corresponds to approximation $V_k = V_{k_F}$). Parameters $\delta_i = \epsilon_i + U_i/2$ measure the departure from the particle-hole (p-h) symmetric point at $\delta_1 = \delta_2 = 0$. The model is schematically depicted in Fig. 1b. In the p-h symmetric point, 2IAM has $\mathrm{SU}(2)_{\mathrm{spin}} \times \mathrm{SU}(2)_{\mathrm{isospin}}$ symmetry like SCKM.

In Fig. 5 we show the spin susceptibility and expectation values of the local charge fluctuations $\Delta n_i^2 = (n_i - \langle n_i \rangle)^2$, inter-impurity charge fluctuations $\Delta n_1 n_2 = (n_1 - \langle n_1 \rangle)(n_2 - \langle n_2 \rangle)$, and the inter-impurity spin correlations $\boldsymbol{S}_1 \cdot \boldsymbol{S}_2$ as a function of the hybridization strength Γ.

For small Γ, i.e. for small equivalent Kondo exchange couplings

$$J_S = \frac{8\Gamma_1}{\pi U_1}, \quad J_C = \frac{8\Gamma_2}{\pi |U_2|}, \tag{23}$$

the first impurity behaves at low temperatures as the SIAM with the same U_1, Γ_1, see Fig. 5a. The good agreement at low temperatures demonstrates that spin and charge degrees of freedom in the 2IAM effectively separate in spite of charge fluctuation on the impurity 1 and spin fluctuations on the impurity 2, as discussed above for the case of a single Anderson impurity. At temperatures above the moment formation temperature $T^* \approx 1/5U$[48], the magnetic susceptibility is larger than that of the SIAM model by a factor of 2 as both impurities are then in the free orbital regime with equally probable configurations $|0\rangle, |\uparrow\rangle, |\downarrow\rangle, |\uparrow\downarrow\rangle$.

For increasing Γ/U, the renormalization effect due to the presence of impurity 2 becomes noticeable and the Kondo

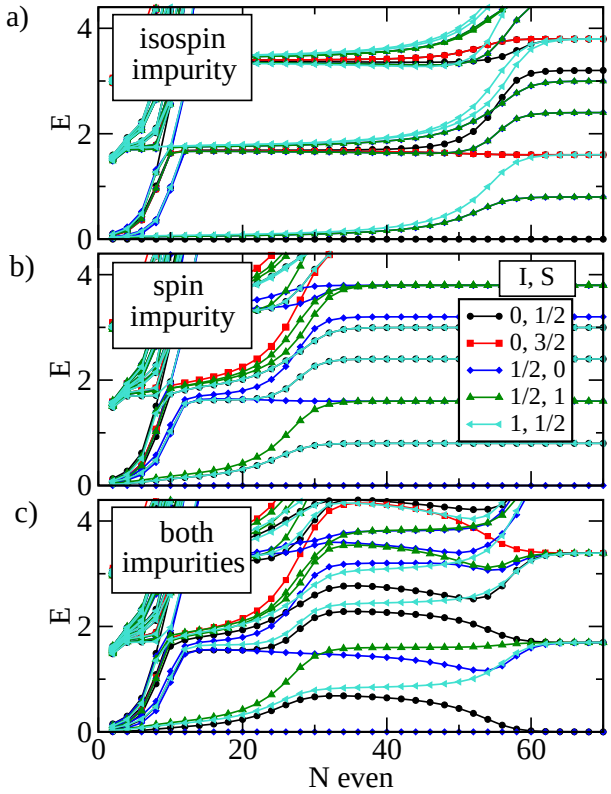

Figure 6: (Color online) Numerical renormalization group eigenvalue flows for the case when a) isospin impurity only, b) spin impurity only, c) both impurities are present. $U_1 = U = 0.01$, $\Gamma, 1, 2/U = 0.05$ (unless turned to zero in a and b), $U_2 = -3U$. The levels are labeled by the total isospin and spin quantum numbers, (I, S).

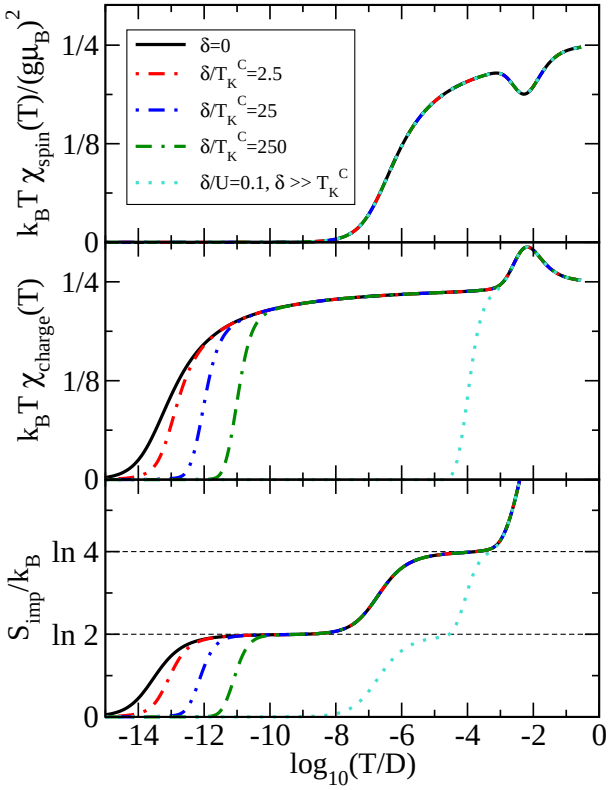

Figure 7: (Color online) Impurity susceptibilities and entropy for the two-impurity Anderson model. Impurity 1 has $U_1 = U = 0.01$, $\Gamma/U = 0.05$. Impurity 2 has $U_2 = -3U = -0.03$ and equal hybridization Γ. $T_K^S/D \sim 1.1\ 10^{-6}$, $T_K^C/D \sim 2.9\ 10^{-13}$. Note that the magnetic susceptibility curves nearly overlap for all values of δ.

temperature is lower than in the corresponding SIAM model. This can again be explained in terms of Kondo cloud "stiffness", see Sec. III. For very large Γ/U we observe an interesting saturation effect. While for $U/\pi\Gamma < 1$ the Kondo effect in SIAM collapses, charge fluctuations rise to the maximum value of $\Delta n^2 = 0.5$ and the susceptibility drops to zero at $T \sim \Gamma$[48], in 2IAM the charge fluctuations on impurity 1 are constrained due to the presence of impurity 2 (see the slow rise of the Δn_1^2 curve in Fig. 5b) and, similarly, spin fluctuations on impurity 2 are constrained due to the presence of impurity 1 (see Δn_2^2 curve). The temperature dependence of the susceptibility is in this case approximately $T\chi(T) \sim \log T$ in a temperature interval of four orders of magnitude, with the low-temperature tail still having the form of the universal Kondo curve.

In Fig. 6 we show NRG eigenvalue flows for: a) single $U < 0$ impurity, b) single $U > 0$ impurity and c) the 2IAM with both impurities. It clearly shows the difference between SIAM and 2IAM: for negative-U SIAM the ground state is an isospin singlet and the system is a Fermi liquid with a $\delta_{\rm qp} = \pi/2$ phase shift; for positive-U SIAM the ground state is a spin singlet and the system is a Fermi liquid with a $\delta_{\rm qp} = \pi/2$ phase shift; finally, in the 2IAM the ground state is a spin-singlet isospin-singlet (for odd N; for even N that we show, the finite-size ground state consists of degenerate $I = 1/2, S = 0$, $I = 0, S = 1/2$ states) and the system is a Fermi liquid with zero phase shift as in the SCKM model, see Sec. VI.

The departure from the p-h symmetric point is a marginal perturbation for the positive-U impurity and, as long as $|\delta_1| \lesssim U/2$, the spin Kondo effect persists[48]. The p-h symmetry breaking is, however, a relevant perturbation for the negative-U impurity, where it plays the same role as a magnetic field for the positive-U case (see Sec. II A). If $|\delta_2| > T_K^C$, the charge Kondo effect is washed out. This is illustrated in Fig. 7, where we plot the thermodynamic quantities for a range of $\delta = \delta_1 = \delta_2$. It should be noticed that the spin susceptibility is hardly affected; the curves nearly overlap. The effect of a magnetic field is analogous: it washes out the spin Kondo effect, but it is marginal for the charge Kondo effect.

In Fig. 7 we observe some high temperature features in the thermodynamic properties at $T \sim U_1, U_2$, e.g., a dip in the spin susceptibility and a peak in the charge susceptibility. This is a common feature of the 2IAM models with $U_1 \neq -U_2$. In a single impurity model with $U_1 > 0$, the spin susceptibility increases at the local moment formation temperature $T_1^* = 1/5U_1$ from its free orbital value of $1/8$ to the local moment value of $1/4$, while the charge susceptibility sharply

drops to zero as the charge fluctuations are frozen out. In a single impurity model with $U_2 < 0$ the same scenario occurs at $T_2^* = 1/5|U_2|$ with the spin and isospin sectors exchanged. Therefore, in 2IAM with $U_1 < |U_2|$, as in this case, we observe a dip in the spin susceptibility and a peak in the charge susceptibility, since the pairing moment begins to form at a higher temperature than the magnetic moment. For $U_1 > |U_2|$, there is a peak in the spin susceptibility and a dip in the charge susceptibility. Finally, for $U_1 = -U_2$, magnetic and pairing moments are formed at the same temperature and the variations in $\chi_{\rm spin}$ and $\chi_{\rm charge}$ are hardly visible.

VIII. SPECTRAL DENSITIES AND CONDUCTANCE

Using NRG one can calculate the frequency dependence of the single-particle spectral densities[61,62,63,64], which determine the conductance through a deformable molecule with spin and charge degrees of freedom. We make a simplifying assumption that the molecule described by 2IAM is symmetrically embedded between two electrodes, so that the conduction channel in the model corresponds to the symmetric combination of electrons from both electrodes[65]. The coupling is then proportionate and we may use the Meir-Wingreen formula for the conductance[66]

$$G = G_0 \int_{-\infty}^{\infty} \frac{\partial f}{\partial \omega} \mathrm{Im}[\mathrm{Tr}\{\mathbf{\Gamma G}^r\}] d\omega, \tag{24}$$

where $G_0 = 2e^2/h$ is the conductance quantum, f the Fermi-Dirac distribution function, $\mathbf{\Gamma}$ the hybridization matrix and $\mathbf{G}^r$ the retarded Green's function matrix. The components of the hybridization matrix are

$$\Gamma_{i,j} = \pi \rho(\omega) V_i(\omega) V_j^*(\omega), \tag{25}$$

where V_n is the hopping amplitude from the impurity orbital n to the conduction band. In a simplified model we assume a constant density of states ρ and an energy-independent hybridization strength $\Gamma = \pi \rho_0 |V|^2$ which is the same for both orbitals. All components of the hybridization matrix are then the same: $\Gamma_{ij} = \Gamma$. Equation (24) simplifies to

$$G = G_0 \int_{-\infty}^{\infty} \left(-\frac{\partial f}{\partial \omega} \right) \pi \Gamma \sum_{ij} \mathrm{Im} \left(-\frac{1}{\pi} G_{ij}^r \right) d\omega. \tag{26}$$

The quantity in the parenthesis is related to the spectral density matrix for both orbitals, $A_{ij} = -1/(2\pi)\mathrm{Im}(G_{ij}^r + G_{ji}^r)$. It can be computed using standard NRG techniques from matrix elements of the creation operators using the following spectral decompositions:

$$\begin{aligned} A_{i,j}(\omega > 0) &= \frac{1}{Z} \sum_{m,n_0} \mathrm{Re} \left[\left(\langle m | d_i^\dagger | n_0 \rangle \right)^* \langle m | d_j^\dagger | n_0 \rangle \right] \\ &\quad \times \delta(\omega - E_m), \\ A_{i,j}(\omega < 0) &= \frac{1}{Z} \sum_{m_0,n} \mathrm{Re} \left[\left(\langle m_0 | d_i^\dagger | n \rangle \right)^* \langle m_0 | d_j^\dagger | n \rangle \right] \\ &\quad \times \delta(\omega + E_n), \end{aligned} \tag{27}$$

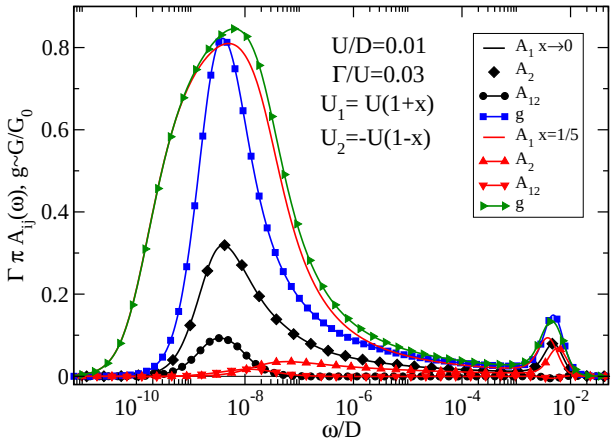

Figure 8: (Color online) Diagonal (A_1, A_2) and out-of-diagonal spectral density (A_{12}) of the two impurity Anderson model for different asymmetry parameters x. We plot only the positive frequencies. Due to the particle-hole symmetry, we have $A_i(\omega) = A_i(-\omega)$ and $A_{12}(\omega) = -A_{21}(-\omega)$.

where Z is the spectral sum $Z = \mathrm{Tr}(e^{-\beta H})$, indices m_0, n_0 with subscript 0 run over (eventually degenerate) ground states and indices m, n without a subscript over all states. Delta functions need to be appropriately broadened[67]. Note that there is a sum rule

$$\int_{-\infty}^{\infty} A_{ij}(\omega) d\omega = \delta_{ij}, \tag{28}$$

which follows from the fermionic anti-commutation relation $a_{i\mu}^\dagger a_{j\mu} + a_{j\mu} a_{i\mu}^\dagger = \delta_{ij}$.

We are particularly interested in the symmetrized and normalized spectral density function $g(\omega)$ defined by

$$g(\omega) = \pi \Gamma \sum_{ij} A_{ij}(\omega) \tag{29}$$

where $i, j = 1, 2$. This quantity appears in the final expression for the conductance:

$$G = G_0 \int_{-\infty}^{\infty} \left(-\frac{\partial f(\omega)}{\partial \omega} \right) g(\omega) d\omega. \tag{30}$$

In a simple approximation, the temperature dependence of the conductance through the quantum dots can be deduced from the energy dependence of the function $g(\omega)$.

We computed the spectral densities $A_i(\omega) = A_{ii}(\omega)$ and the out-of-diagonal spectral density $A_{12}(\omega)$ for a constant Γ and a range of U_1, U_2, defined by $U_1 = U(1+x)$ and $U_2 = -U(1-x)$ with constant U, see Fig. 8. For $x = 0$, the Kondo temperatures are the same.

In the generic case $x \neq 0$ (assuming $x > 0$, so that $T_K^S > T_K^C$), the spectral density of the first impurity increases for $\omega \lesssim T_K^S$, but then it drops to zero for $\omega \lesssim T_K^C$, see the case of $x = 1/5$. We thus obtain a peak centered at $\omega \sim \sqrt{T_K^S T_K^C}$. This is at first surprising, since spin Kondo effect is usually associated with an Abrikosov-Suhl resonance at zero frequency

in the spectral density and, due to the spin-charge decoupling, one would expect no influence of the charge Kondo effect induced by the second impurity. Indeed, at low temperatures the thermodynamic functions related to spin are universal functions of T_K^S only; for example, $\chi_{\rm spin}$ in no way depends on the charge Kondo temperature T_K^C. There is clearly no such universality in the dynamic quantities. Spectral density is related to the injection of a physical fermion in the system; the fermion carries both spin and isospin degrees of freedom and is therefore sensitive to both sectors.

For relatively large $x = 1/5$, the spectral density on the second impurity, $A_2(\omega)$, has a small bulge at T_K^S and then it drops to zero. We emphasize that no Abrikosov-Suhl resonance appears in $A_2(\omega)$ below T_K^C as might be expected. For x tending towards 0, the bulge in $A_2(\omega)$ develops into a peak of the same form as the one found in $A_1(\omega)$. The out-of-diagonal spectral density $A_{12}(\omega)$ also builds up a small peak at $\omega \sim T_K$ as $x \to 0$ and goes to zero at low frequencies for all x. These results indicate that the temperature dependence of conductance is expected to be non-monotonic: it begins to increase at the higher of the two Kondo temperatures, but then it decreases when the lower Kondo temperatures is reached. The system does not conduct at zero temperature, $g(\omega \to 0) = 0$. This results is consistent with the zero temperature conduction of Fermi liquids as determined by the quasiparticle phase shift $\delta_{\rm qp} = 0$:

$$G(T = 0) = G_0 \sin^2 \delta_{\rm qp} = 0. \tag{31}$$

The effect of the gate voltage δ is shown in Fig. 9 for the case of widely separated spin and charge Kondo temperatures, $T_K^C \ll T_K^S$ (see also Fig. 7 where the thermodynamic properties are shown for the same parameters). For $\delta > T_K^C$, the isospin fluctuations on the second orbital are rapidly quenched and the isospin degree of freedom is fully polarized [see $A_2(\omega)$]. The low-frequency peak in the spectral density on the first orbital is restored at the same time. It should be noted that the out-of-diagonal spectral density $A_{12}(\omega)$ is small for all δ. With increasing δ, the conductance thus rises from zero toward the unitary limit

$$G(\delta \gg T_K^C) \approx G_0. \tag{32}$$

We consider the significance of such behavior in the conclusion.

IX. TWO-IMPURITY ANDERSON-HOLSTEIN MODEL

In previous sections, we performed calculations using the 2IAM with a negative U_2 parameter that we considered as a given constant. In this section we first study how an effective negative U_2 emerges in the presence of the charge-phonon coupling (Anderson-Holstein model) and then extend this model to the two impurity case with one Anderson impurity (spin degree of freedom) and one Holstein impurity (isospin degree of freedom).

The Anderson-Holstein model is an extension of the Holstein model in that it considers electrons with spin and (optionally) a finite on-site electron-electron repulsion in the impurity[14], see Fig. 1c. The Hamiltonian is

$$\begin{aligned} H = &\sum_{k\sigma} \epsilon_k c^\dagger_{k\sigma} c_{k\sigma} + \sum_{k\sigma} V_k \left(d^\dagger_\sigma c_{k\sigma} + \text{H.c.} \right) \\ &+ U(n-1)^2 + g(a^\dagger + a)(n-1) + \omega_0 a^\dagger a \end{aligned} \tag{33}$$

where d is the electron annihilation operator on the impurity and a is the annihilation operator for a phonon of frequency ω_0 which couples to the charge $n = \sum_\sigma d^\dagger_\sigma d_\sigma$ with electron-phonon (e-ph) coupling strength g. The phonon does not break the particle-hole symmetry, however the full isospin $\mathrm{SU}(2)_{\rm isospin}$ symmetry is reduced to $\mathrm{U}(1)_{\rm charge}$ conservation of charge symmetry.

In general, the phonon renormalizes both the e-e interaction U, which becomes frequency dependent, and the hybridization strength Γ. In the anti-adiabatic limit $\omega_0 \gg U$, the effective e-e interaction again becomes instantaneous and the Anderson-Holstein model maps to the usual single impurity Anderson model (SIAM) with[14]

$$U_{\rm eff} = U - 2g^2/\omega_0. \tag{34}$$

For large enough g, $U_{\rm eff}$ becomes negative and the charge Kondo effect is expected. In this limit ($\omega_0 \gg U$), the effective exchange interaction for the isospin degrees of freedom is isotropic[22] and the $\mathrm{SU}(2)_{\rm isospin}$ symmetry is largely restored at energies much lower than ω_0.

The reversal of roles of spin and charge fluctuations in the Anderson-Holstein model was first deduced from dynamic spin and charge susceptibilities at zero temperature in Ref. 14. In Fig. 10 we demonstrate this reversal in the temperature dependent thermodynamic spin and charge susceptibilities where the disappearance of the magnetic moment and emergence of the pairing moment is explicit.

When the Coulomb repulsion in an orbital is small, $U \to 0$, but the coupling to a phonon mode is substantial, we have $U_{\rm eff} = -2g^2/\omega_0$. This holds *exactly* in this case (i.e. the condition $\omega_0 \gg U$ is trivially met). If, however, U and ω_0 in the same orbital are of the same magnitude, or $U \gg \omega_0$, the appropriate mapping is to the anisotropic Kondo model[15,28]. In such systems the charge Kondo temperature is generally strongly attenuated, therefore in this work we do not discuss the case $U \gtrsim \omega_0$ further.

As an illustration, we now consider the case of two active orbitals, the first with $U_1 > 0$ and the second with $U_2 = 0$ and a phonon mode, as schematically depicted in Fig. 1d. The Hamiltonian of this two-impurity Anderson-Holstein model in the particle-hole symmetric point is

$$\begin{aligned} H = &\sum_{k\sigma} \epsilon_k c^\dagger_{k\sigma} c_{k\sigma} \\ &+ U_1(n_1 - 1)^2 + g(a^\dagger + a)(n_2 - 1) + \omega_0 a^\dagger a \\ &+ \sum_{k\sigma} V^1_k \left(d^\dagger_{1\sigma} c_{k\sigma} + \text{H.c.} \right) + \sum_{k\sigma} V^2_k \left(d^\dagger_{2\sigma} c_{k\sigma} + \text{H.c.} \right). \end{aligned} \tag{35}$$

The presence of the phonon degrees of freedom greatly increases the degeneracy and thus the number of states that need

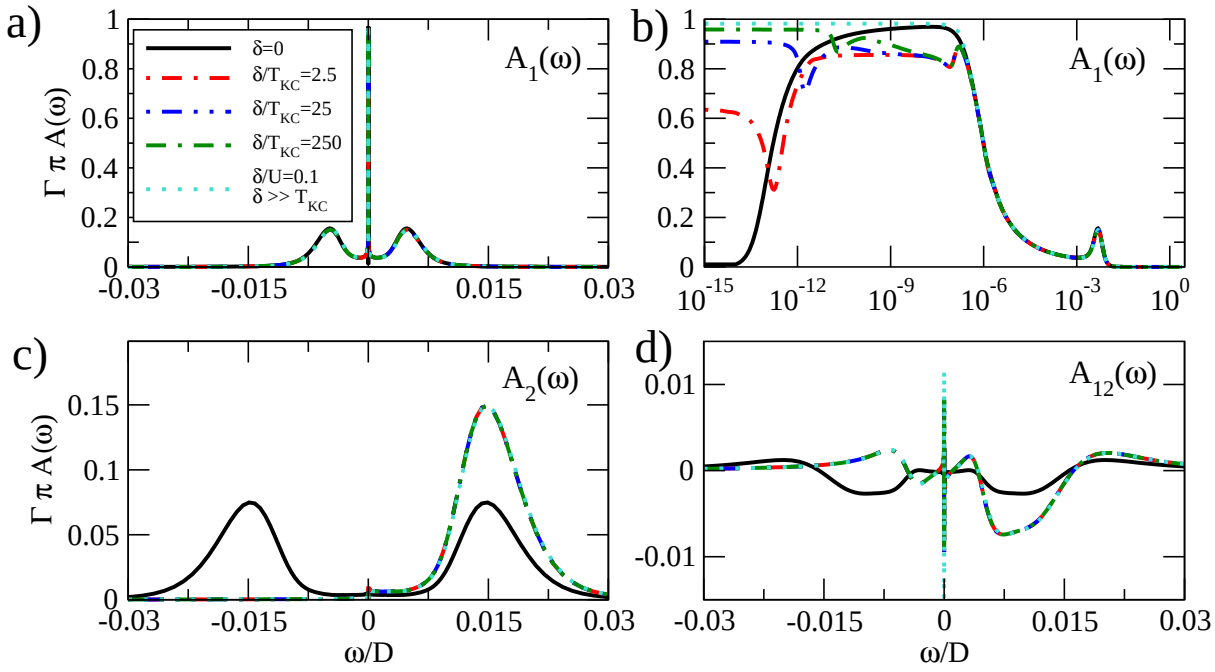

Figure 9: (Color online) Diagonal (A_1, A_2) and out-of-diagonal spectral densities (A_{12}) of the two impurity Anderson model. Same parameters as in Fig. 7.

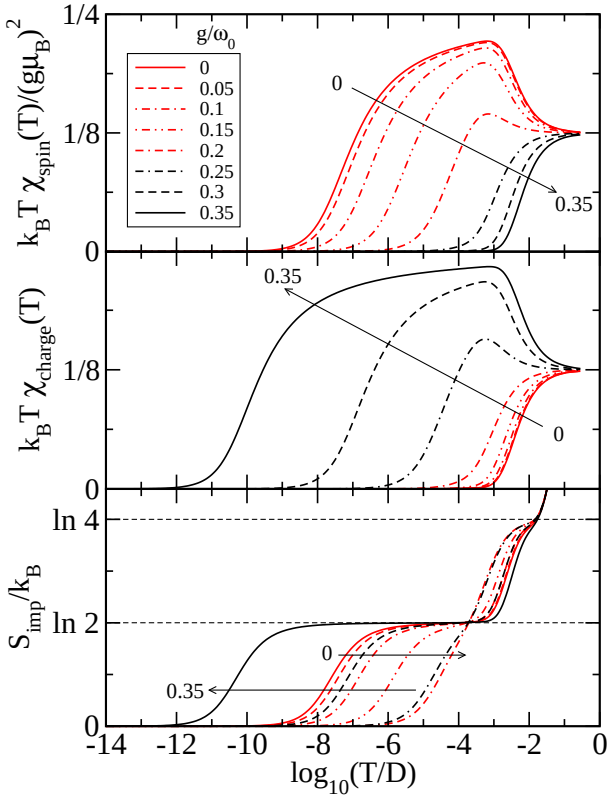

Figure 10: (Color online) Impurity susceptibilities and entropy for the single-impurity Anderson-Holstein model for increasing e-ph interaction strength g. $U/D = 0.01$, $\Gamma/U = 0.04$, $\omega_0/D = 0.1$.

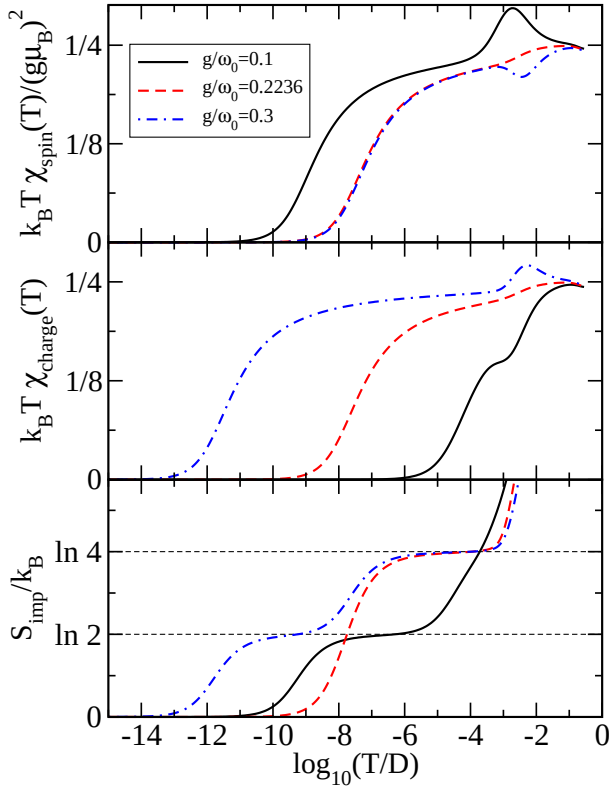

Figure 11: (Color online) Impurity susceptibilities and entropy for the two-impurity model with one Holstein impurity with $\omega_0/D = 0.1$ and varying e-ph interaction strength g, and one Anderson impurity with $U/D = 0.01$. Both impurities are coupled with $\Gamma/D = 0.0004$ to the conduction band.

to be kept in the truncation step of the NRG[47]. We used discretization parameter $\Lambda = 3$, the discretization scheme of Ref. 52, and we took into account the $\mathrm{SU}(2)_{\mathrm{spin}}$ and $\mathrm{U}(1)_{\mathrm{charge}}$ symmetries. We used $\beta = 0.75$[47,48]. We kept up to 5000 states (not taking into account the degeneracies) or the states with energy below $15T_N$, whichever number is lower. In addition, since the eigenvalues in NRG are clustered, we took care not to truncate in the middle of a cluster, so that we do not introduce systematic errors. This approach gives converged results which agree for several values of the parameter z used.

For finite g, a pairing moment is induced in the first orbital and a magnetic moment in the second: we then expect a simultaneous spin and charge Kondo effect, as in the two-impurity Anderson model. This is confirmed by the results for the thermodynamic properties in Fig. 11. For small $g/\omega_0 = 0.1$, U_{eff} is small and hence the effective isospin exchange constant J_C is large: the magnetic exchange constant J_S is then renormalized and the spin Kondo temperature is reduced, as described in Sec. III. As g is increased, the charge Kondo temperature rapidly decreases, while the spin Kondo temperature returns to its unrenormalized value. At a particular value of $g/\omega_0 = \sqrt{U/(2\omega_0)} = 0.2236$, the spin and charge Kondo temperatures are the same.

X. CONCLUSION AND DISCUSSION

We have studied the degree of the spin-charge separation in single-channel quantum impurity models where the impurity carries both the spin and isospin degrees of freedom. Using numerical renormalization group calculations we have confirmed the well known fact that in the continuum limit, i.e. when the band-width D is much larger than all other relevant scales in the problem, spin and isospin degrees of freedom of a single conduction band behave as two decoupled and independent spin-$1/2$ $\mathrm{SU}(2)$ degrees of freedom subject only to gluing conditions. This implies that the spin and charge Kondo effects can coexist, the demonstration of which is the main result of our work. When D is comparable to other scales, lattice effects become important since a single orbital cannot sustain a spin and isospin moment at the same time. The separate screening of spin and isospin degrees of freedom exists even in this limit, but the corresponding Kondo temperatures are reduced compared to the single-impurity results due to the renormalization of the Kondo exchange constants.

We have explored the model of a deformable molecule with two active orbitals, one carrying a local magnetic moment (described by the Anderson model) and one coupled to a strong phonon mode which induces local pairing moment (described by the Holstein model). We have shown that in the generic case the conductance through such a molecule at the particle-hole symmetric case has non-uniform temperature dependence: it rises at the higher of the two Kondo temperatures, but then drops to zero below the lower Kondo temperature. By changing the gate voltage from its value at the particle-hole symmetric point, the charge Kondo effect is quenched and the conductance increases back to the unitary limit if the spin Kondo temperature is much higher than the charge Kondo temperature, $T_K^S \gg T_K^C$. Conversely, the magnetic field can be used to quench the spin Kondo effect and the conductance attains the unitary limit if $T_K^C \gg T_K^S$. Detection of such behavior could serve as an experimental probe of the simultaneous spin and charge Kondo effect. The spin-charge Kondo effect occurs only around the particle-hole symmetric point (i.e. for precisely tuned gate voltage) and zero magnetic field. In the case of widely separated charge and spin Kondo temperatures, it would thus appear as a small region of zero or reduced conductance within a wider region of the high conductance "Kondo plateau" when plotted as a function of the gate voltage and the magnetic field. In the case of similar charge and spin Kondo temperatures, it would be difficult to distinguish (at constant low temperature) the zero conductance due to simultaneous charge and spin Kondo effects from the Coulomb-blockade valley. The temperature dependence of the conductance is, however, different. In the case of Coulomb blockade, conductance monotonously decreases below the temperature scale of charge excitations. In the case of simultaneous charge and spin Kondo effects, the decrease due to Coulomb blockade is followed by increasing conductance that peaks at the Kondo temperature before it goes to zero.

Acknowledgments

The authors acknowledge the financial support of the SRA under Grant No. P1-0044.

[1] L. H. Yu and D. Natelson, Nanoletters **4**, 79 (2004).
[2] L. H. Yu, Z. K. Keane, J. W. Ciszek, L. Cheng, M. P. Stewart, J. M. Tour, and D. Natelson, Phys. Rev. Lett. **93**, 266802 (2004).
[3] L. H. Yu, Z. K. Keane, J. W. Ciszek, L. Cheng, J. M. Tour, T. Baruah, M. R. Pederson, and D. Natelson, Phys. Rev. Lett. **95**, 256803 (2005).
[4] H. Park, J. Park, A. K. L. Lim, E. H. Anderson, A. P. Alivisatos, and P. L. McEuen, Nature **407**, 57 (2000).
[5] J. Park, A. N. Pasupathy, J. I. Goldsmith, C. Chang, Y. Yaish, J. R. Petta, M. Rinkoski, J. P. Sethna, H. D. Abruna, P. L. McEuen, et al., Nature **417**, 722 (2002).
[6] W. Liang, M. P. Shores, M. Bockrath, J. R. Long, and K. Park, Nature **417**, 725 (2002).
[7] A. N. Pasupathy, R. C. Bialczak, J. Martinek, J. E. Grose, L. A. K. Donev, P. L. McEuer, and D. C. Ralph, Science **306**, 86 (2004).
[8] P. Wahl, L. Diekhoner, G. Wittich, L. Vitali, M. A. Schneider, and K. Kern, Phys. Rev. Lett. **95**, 166601 (2005).
[9] B. C. Stipe, M. A. Rezaei, and W. Ho, Science **280**, 1732 (1998).
[10] J. R. Hahn and W. Ho, Phys. Rev. Lett. **87**, 196102 (2001).
[11] A. C. Hewson and D. M. Newns, J. Phys. C **13**, 4477 (1980).
[12] A. C. Hewson, J. Phys. C: SOlid State Phys. **14**, 2747 (1981).
[13] D. Meyer, A. C. Hewson, and R. Bulla, Phys. Rev. Lett. **89**,

196401 (2002).
[14] A. C. Hewson and D. Meyer, J. Phys. - Condens. Mat. **14**, 427 (2002).
[15] P. S. Cornaglia, H. Ness, and D. R. Grempel, Phys. Rev. Lett. **93**, 147201 (2004).
[16] J. Mravlje, A. Ramšak, and T. Rejec, Phys. Rev. B **72**, 121403(R) (2005).
[17] G. S. Jeon, T.-H. Park, and H.-Y. Choi, Phys. Rev. B **68**, 045106 (2003).
[18] H. C. Lee and H.-Y. Choi, Phys. Rev. B **69**, 075109 (2004).
[19] H. C. Lee and H.-Y. Choi, Phys. Rev. B **70**, 085114 (2004).
[20] P. S. Cornaglia and D. R. Grempel, Phys. Rev. B **71**, 245326 (2005).
[21] J. Koch, M. E. Raikh, and F. von Oppen, Phys. Rev. Lett. **96**, 056803 (2006).
[22] M.-J. Hwang, M.-S. Choi, and R. Lopez, *Pair tunneling and shot noise through molecular transistors*, cond-mat/0608599 (2006).
[23] P. S. Cornaglia, D. R. Grempel, and H. Ness, Phys. Rev. B **71**, 075320 (2005).
[24] K. A. Al-Hassanieh, C. A. Busser, G. B. Martins, and E. Dagotto, Phys. Rev. Lett. **95**, 256807 (2005).
[25] C. A. Balseiro, P. S. Cornaglia, and D. R. Grempel, *Electron-phonon correlation effects in molecular transistors*, cond-mat/0605064 (2006).
[26] A. Taraphder and P. Coleman, Phys. Rev. Lett. **66**, 2814 (1991).
[27] B. A. Jones, C. M. Varma, and J. W. Wilkins, Phys. Rev. Lett. **61**, 125 (1988).
[28] H.-B. Schuttler and A. J. Fedro, Phys. Rev. B **38**, 9063 (1988).
[29] I. Affleck, Nucl. Phys. B **336**, 517 (1990).
[30] J. Voit, Rep. Prog. Phys. **57**, 977 (1995).
[31] B. J. Kim, H. Koh, E. Rotenberg, S.-J. Oh, H. Eisaki, N. Motoyama, S. Uchida, T. Tohyama, S. Maekawa, Z.-X. Shen, et al., Nature Phys. **2**, 397 (2006).
[32] O. M. Auslaender, H. Steinberg, A. Yacoby, Y. Tserkovnyak, B. I. Halperin, K. W. Baldwin, L. N. Pfeiffer, and K. W. West, Science **308**, 88 (2005).
[33] G. Zarand and J. von Delft, Phys. Rev. B **61**, 6918 (2000).
[34] J. von Delft, G. Zarand, and M. Fabrizio, Phys. Rev. Lett. **81**, 196 (1998).
[35] M. Blume, V. J. Emery, and A. Luther, Phys. Rev. Lett. **25**, 450 (1970).
[36] P. Coleman, L. B. Ioffe, and A. M. Tsvelik, Phys. Rev. B **52**, 6611 (1995).
[37] L. I. Glazman, F. W. J. Hekking, and A. I. Larkin, Phys. Rev. Lett. **83**, 1830 (1999).
[38] D. Goldhaber-Gordon, H. Shtrikman, D. Mahalu, D. Abusch-Magder, U. Meirav, and M. A. Kastner, Nature **391**, 156 (1998).
[39] A. C. Hewson, *The Kondo Problem to Heavy-Fermions* (Cambridge University Press, Cambridge, 1993).
[40] Y. Nambu, Phys. Rev. **117**, 648 (1960).
[41] P. W. Anderson, Phys. Rev. **112**, 1900 (1958).
[42] I. Affleck, A. W. W. Ludwig, H.-B. Pang, and D. L. Cox, Phys. Rev. B **45**, 7918 (1992).
[43] J. Ye, Nucl. Phys. B **512**, 543 (1998).
[44] S. C. Bradley, R. Bulla, A. C. Hewson, and G.-M. Zhang, Eur. Phys. J. B **11**, 535 (1999).
[45] R. Bulla, A. C. Hewson, and G.-M. Zhang, Phys. Rev. B **56**, 11721 (1997).
[46] P. Coleman and A. J. Schofield, Phys. Rev. Lett. **75**, 2184 (1995).
[47] K. G. Wilson, Rev. Mod. Phys. **47**, 773 (1975).
[48] H. R. Krishna-murthy, J. W. Wilkins, and K. G. Wilson, Phys. Rev. B **21**, 1003 (1980).
[49] F. D. M. Haldane, J. Phys. C: Solid State Phys. **14**, 2585 (1981).
[50] M. G. Zacher, E. Arrigoni, W. Hanke, and J. R. Schrieffer, Phys. Rev. B **57**, 6370 (1998).
[51] K. V. Samokhin, J. Phys.: Condens. Matter **10**, L533 (1998).
[52] V. L. Campo and L. N. Oliveira, Phys. Rev. B **72**, 104432 (2005).
[53] R. Bulla, T. Pruschke, and A. C. Hewson, J. Phys.: Codens. Matter. **9**, 10463 (1997).
[54] R. Žitko and J. Bonča, Phys. Rev. B **74**, 045312 (2006).
[55] I. Affleck and A. W. W. Ludwig, Nucl. Phys. B **352**, 849 (1991).
[56] I. Affleck, A. W. W. Ludwig, and B. A. Jones, Phys. Rev. B **52**, 9528 (1995).
[57] T.-S. Kim, L. N. Oliveira, and D. L. Cox, Phys. Rev. B **55**, 12460 (1997).
[58] P. Goddard and D. Olive, Int. J. Mod. Phys. A **1**, 303 (1986).
[59] P. W. Anderson, Phys. Rev. **124**, 41 (1961).
[60] J. R. Schrieffer and P. A. Wolff, Phys. Rev. **149**, 491 (1966).
[61] T. A. Costi and A. C. Hewson, J. Phys. - Cond. Mat. **5**, L361 (1993).
[62] T. A. Costi, A. C. Hewson, and V. Zlatic, J. Phys.: Condens. Matter **6**, 2519 (1994).
[63] W. Hofstetter, Phys. Rev. Lett. **85**, 1508 (2000).
[64] T. A. Costi, Phys. Rev. B **64**, 241310(R) (2001).
[65] L. I. Glazman and M. E. Raikh, JETP Lett. **47**, 452 (1988).
[66] Y. Meir and N. S. Wingreen, Phys. Rev. Lett. **68**, 2512 (1992).
[67] R. Bulla, T. A. Costi, and D. Vollhardt, Phys. Rev. B **64**, 045103 (2001).
[68] In fact, $\boldsymbol{J}^S(x)$ and $\boldsymbol{J}^C(x)$ are spin and isospin *densities*, but we will use the conventional CFT nomenclature.